A Prototype X-ray Framing Camera With Variable Exposure Time Based on Double-Gated Micro-Channel Plates

Wenzheng Yang, Xun Hou, Yonglin Bai, Xiaohong Bai, Baiyu Liu, Junping Zhao, and Junjun Qin

Abstract—We present a novel X-ray frame camera with variable exposure time that is based on double-gated micro-channel plates (MCP). Two MCPs are connected so that their channels form a Chevron-MCP structure, and four parallel micro-strip lines (MSLs) are deposited on each surface of the Chevron-MCP. The MSLs on opposing surfaces of the Chevron-MCP are oriented normal to each other and subjected to high voltage. The MSLs on the input and output surfaces are fed high voltage pulses to form a gating action. In forming two-dimensional images, modifying the width of the gating pulse serves to set exposure times (ranging from ps to ms) and modifying the delay between each gating pulse serves to set capture times. This prototype provides a new tool for high-speed X-ray imaging, and this paper presents both simulations and experimental results obtained with the camera.

Index Terms—High speed imaging, microchannel plate (MCP), multi-framing camera, x-ray diagnosis.

I. INTRODUCTION

-RAY FRAMING CAMERAS (XFC) based on microchannel plates (MCP) (abbr. MCP-XFC) are used in a wide variety of scientific fields [1]–[6], including inertial confinement fusion (ICF), laser-produced plasmas, Z-pinch plasma confinement, and photo-physics. This type of framing camera typically consists of a proximity-focused MCP framing tube containing a phosphor screen and a micro-strip line (MSL) cathode on the MCP's input surface, a control unit (including an electrical pulse generator), and recording equipment. In this type of high-speed imaging system, the MCP serves as a gated two-dimensional electron multiplier. It is sensitive not only to electrons but also to ions, UV, X-rays and γ -rays. MCPs offer a unique combination of attractive properties such as high gain and high spatial resolution, making them useful in a wide range of detection applications.

Manuscript received April 06, 2008; revised August 10, 2008, November 15, 2008, December 27, 2008, and February 09, 2009. Current version published August 12, 2009. This work was supported by the National Natural Science Foundation of China under Grants 10376041 and 60777027.

W. Yang, X. Hou, Y. Bai, and B. Liu are with State Key Laboratory of Transient Optics and Photonics, Xi'an Institute of Optics and Precision Mechanics, Chinese Academy of Sciences, Xi'an 710119, China (e-mail: ywz@opt.ac.cn; houxun@opt.ac.cn; baiyonglin@opt.ac.cn; liubaiyu@opt.ac.cn).

X. Bai, J. Zhao, and J. Qin are with Key Laboratory of Ultrafast Photoelectric Diagnostics Technology, Xi'an Institute of Optics and Precision Mechanics, Chinese Academy of Science, Xi'an 710119, China (e-mail: bhx@opt.ac.cn; junping.zhao@opt.ac.cn; qjj@opt.ac.cn).

Digital Object Identifier 10.1109/TNS.2009.2025176

The MSL cathode is a microwave transmission line deposited on the input surface of the MCP and is sensitive to X-rays. This transmission line is designed to allow high frequency, high voltage (HV) electrical pulses (10 GHz and 1–3 kV) to propagate along the line that serve to gate the MCP. The MCP-XFC system is also equipped with a pinhole array and its adjusting mechanism.

To record a time-resolved X-ray image, the pinhole array focuses several X-ray images of an object on different parts of the MSL photocathode. The photocathode, gated by the electrical pulses, converts these X-ray images into their corresponding electron images. The gated electron images are in turn converted into optical images by the phosphor screen, so that several two-dimensional images with identical exposure times but captured at different times, appear on the phosphor screen to be recorded by the CCD camera.

Several multi-framing cameras using MCPs with multiple gold MSLs (Au-MSLs) have been reported [4]–[9]. Some of them are used for ICF research, which requires a temporal resolution <100 ps, a spatial resolution of approximately 10 μ m, and a total camera working time of 1–2 ns. Others are used for research with Z-pinch and laser-produced plasmas, requiring only nanosecond-scale temporal resolution but a total camera working time from microseconds to milliseconds.

Typically, the MCP framing tube consists of one gated MCP or an assembly of double-MCPs in contact to form a Chevron-MCP structure. The Au-MSLs are deposited on the input surface of the first MCP (MCP_1) while a metal electrode is deposited on the entire output surface of the second MCP (MCP_2) . In this scenario, the second MCP serves only as an electron multiplier to increase the gain of the tube. Such a structure is referred to as a single-gated Chevron-MCP-XFC.

In 1995, Chang *et al.* reported a picosecond XFC based on a Chevron-MCP which has four Au-MSLs on both its input and output surfaces [10]. In this XFC, the photoelectron image is gated in cascade by two MSLs; one on MCP₁ and another on MCP₂. The MSLs on the input and output surfaces are oriented parallel to each other, which we call a "parallel doublegated Chevron-MCP-XFC". By adjusting the pulse width and the delay time between the gating pulses on the input and output Au-MSLs, the temporal resolution of the camera can be varied. However, the temporal intervals between images on one pair of Au-MSLs are fixed values (on the order of picoseconds). The precise value depends on the space between the images and the propagation velocity of the high voltage (HV) pulses along the MSLs.

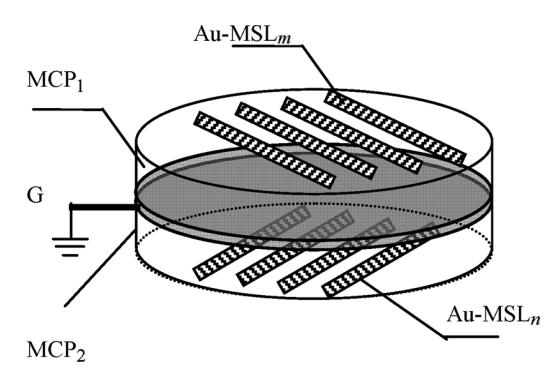


Fig. 1. Schematic diagram of the orthogonal double-gated Chevron-MCP structure. Two MCPs are contacted to each other so that their channels form Chevron structures. Four parallel Au-MSLs (6-mm width and 3-mm spacing) are deposited on the input surface and four on the output surface of the Chevron MCP. The MSLs on the two surfaces of the Chevron-MCP are oriented normal to each other. Gold is evaporated onto the output surface of MCP1 and the input surface of MCP₂ as a common ground electrode (G).

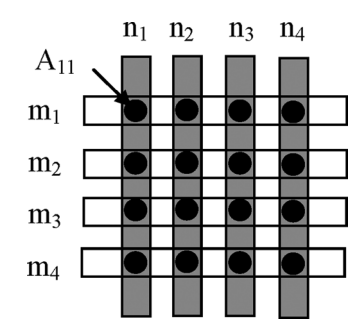


Fig. 2. Projected view of micro-strip lines on both surfaces of the orthogonal double-gated Chevron-MCP structure.

Gated MCP-XFCs are typically constructed from MCPs 0.5-mm thick and 56-mm in diameter, in which case the propagation velocity of the HV pulse along the Au-MSL is approximately 0.18 mm/ps, making the transmission time along the entire MSL fall in the range of 200 to 300 ps. Thus the entire MSL will be in the exposure condition state if a HV pulse of nanosecond or longer duration is applied to it. These gated MCP-XFCs, therefore, can capture multiple images of equal (ps) exposure time on a single MSL, with the different images taken sequentially. They cannot capture multiple images each of which have different exposure times of nanoseconds or longer.

This paper describes a new type of two-dimensional XFC that has variable exposure time from picoseconds to nanoseconds, or even longer.

II. DESIGN OF THE FRAMING TUBE

The schematic diagram of the new XFC based on Chevron-MCPs is shown in Fig. 1. In contrast to the single gated or the parallel double-gated Chevron-MCP-XFC just discussed [2], [5], [10], four $Au - MSL_ms$ (m = 1-4) on the input surface of MCP₁ are perpendicular to the four $Au - MSL_n s$ (n = 1-4) on the output surface of MCP_2 (a top-view is shown in Fig. 2). We refer to this structure as an orthogonal double-gated Chevron MCP XFC.

When a particular pair of MSLs, (e.g., row m_i and column n_i of Fig. 2) is simultaneously biased, the photo-electronic image

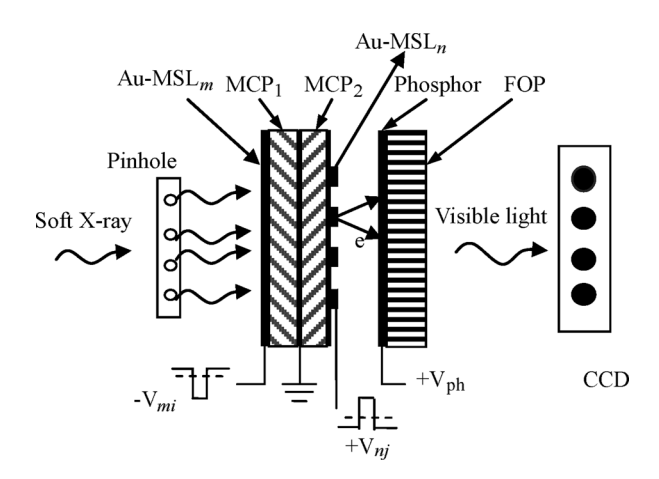


Fig. 3. Schematic illustration of the structure of the orthogonal double-gated Chevron MCP multi-framing camera.

located at the projective orthogonal overlap area, (e.g., A₁₁ in Fig. 2) is gated (i.e., activated) and projected onto the phosphor screen to be recorded by a CCD camera. A schematic diagram of the concept is shown in Fig. 3. By changing the delay times between column pulses V_{ni} , four images on a Au – MSL_m row with different temporal intervals can be obtained. Clearly, the independent control of the gating pulses V_{ni} makes it possible to capture images of a transient process at various time intervals.

In contrast, for the single-gated MCP-XFC or the parallelgated Chevron-MCP-XFC, the four gated images are separated by a fixed time of approximately 50 ps (the precise time delay depends on their spatial separation). Therefore, a phenomenon with tens of ns or μs duration cannot be fully imaged by singlegated MCP-XFC or the parallel double-gated Chevron-MCP-XFC.

III. ANALYSIS AND SIMULATION

For simplicity the electrical pulses are assumed to have Gaussian temporal profiles [11]. In the case, the input gating pulse $V_m(t)$ (with peak value V_{mp} , and FWHM T_m) applied to MCP_1 and the output gating pulse $V_n(t)$ (with peak value V_{nn} , and FWHM T_n) applied to MCP₂ are given as:

$$V_m(t) = V_{mp}e^{\left[-\frac{1}{2}\left(\frac{t}{W_m}\right)^2\right]}$$
 (1-a)

$$V_n(t) = V_{np} e^{\left[-\frac{1}{2}\left(\frac{t}{W_n}\right)^2\right]}$$
 (1-b)

where 2.35 $W_m=T_m$ and 2.35 $W_n=T_n$. If we assume a pulse width of $V_m(t)$ that is much longer than the electron transit time T_{tr} through a micro-channel, then the MCP behaves as if a DC voltage was applied to it and its gain, G, is given by [12]:

$$G = \delta^n = \left(\frac{V}{nV_c}\right)^{k \cdot n}.$$
 (2)

This is the simplest model and represents an MCP with ndynodes where δ is the effective gain per dynode, k is a constant coefficient, and V_c is the so-called first crossover potential. This "dynodized model" [12], [13] neglects the electron transit time spread and the variation of n with voltage.

Defining $G_0 = (1/nV_c)^{\gamma}$ as the initial gain, where $\gamma = k \cdot n$ is a characteristic factor of the MCP, and substituting G_0 and γ into (2), gives:

$$G = G_0 \cdot V^{\gamma}. \tag{3}$$

Equation (3) shows the non-linear relation between the gain ${\cal G}$ and the applied voltage ${\cal V}$.

When MCP_1 is gated by a HV pulse, the gain G is typically given by

$$G_m(t) = G_0 \left[V_m(t) \right]^{\gamma} = G_0 \cdot V_{mp}^{\gamma} \cdot e^{-\frac{1}{2} \left(\frac{t}{(W_m / \sqrt{\gamma})} \right)^2}. \tag{4}$$

There is a narrowing in the FWHM of the gain profile from T_m to $T_m/\sqrt{\gamma}$ for a voltage pulse $V_m(t)$. For $k=0.5, V_c=21.8, n=18.6$ [14], then $\gamma=9.3$ and the initial gain $G_0=e^{(-55.85)}$

The "gain narrowing effect" depends primarily on the shape of the electrical pulse [11]. By analogy, the electron gain of MCP_2 is given by

$$G_n(t) = G_0 \cdot V_{np}^{\gamma} \cdot e^{-\frac{1}{2} \left(\frac{t}{(W_n/\sqrt{\gamma})}\right)^2}.$$
 (5)

If the delay time T_d of the gating pulse on MCP $_2$ relative to the pulse on MCP $_1$ is less than or equal to the transit time T_{tr} of the MCP (i.e., $T_d \leqslant T_{tr}$), the overall gain of the double-gated Chevron-MCP is

$$G_{mn}(t) = G_m(t) \times G_n(t) \tag{6}$$

which has a peak value of

$$G_{mn} = G_0^2 \cdot (V_{mp} \cdot V_{np})^{\gamma} \tag{7}$$

and a FWHM of

$$T_{mn} = \frac{T_m T_n}{\sqrt{\gamma (T_m^2 + T_n^2)}}. (8)$$

Equation (8) indicates that if $T_{\rm m}=T_{\rm n}$, then, due to the non-linear gain effect, the temporal resolution of the double-gated Chevron-MCP-XFC is shorter than that of the single-gated MCP-XFC by a factor of $\sqrt{2}$.

As schematically illustrated in Fig. 4, when an input gating pulse $V_{m1}(t)$ (FWHM = 2.5 ns and $V_{mp}=1$ kV) is applied to $\mathrm{Au}-\mathrm{MSL}_{m1}$ and four output gating pulses $V_{nj}(t)$ (j=1–4) (FWHM = 250 ps and $V_{np}=2$ kV) are applied to $\mathrm{Au}-\mathrm{MSL}_{(n1-n4)}$, with delays of $j\times 500$ ps with respect to $V_{m1}(t)$, then the electronic images from the areas where $\mathrm{Au}-\mathrm{MSL}_{(n1-n4)}$ overlap with $\mathrm{Au}-\mathrm{MSL}_{m1}$ will be created

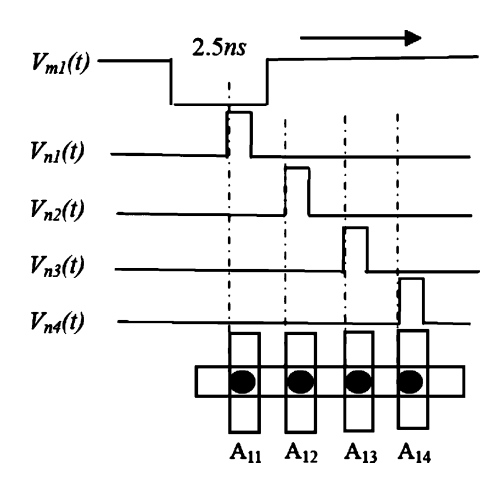


Fig. 4. Timeline diagram of the gating program of images.

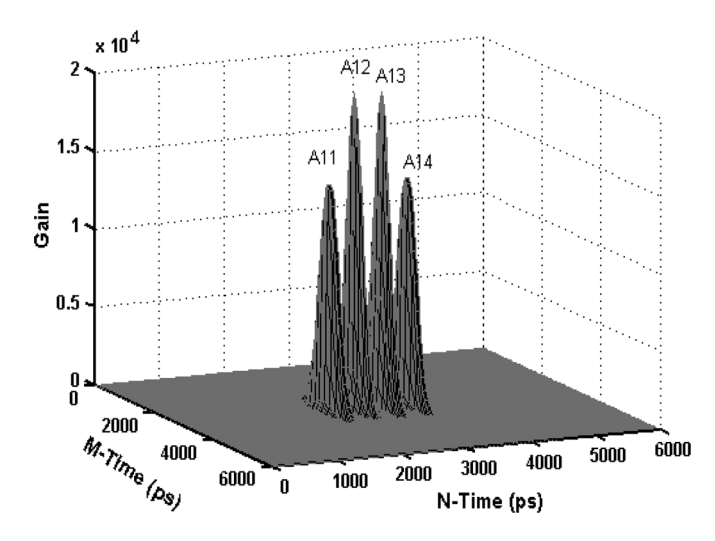


Fig. 5. Electron gains of four gated areas along a $\mathrm{Au}-\mathrm{MSL}_m$ gated with a 2.5 ns-pulse when four 250-ps gating pulses are applied to the orthogonal Au-MSLs n_j (j=1–4). The delay time between two n_j gating pulses is 500 ps.

sequentially and projected onto the phosphor screen. Three-dimensional plots of gain distributions of these gated areas were obtained by numerical stimulation and are shown in Fig. 5. The peak gains of the different gated areas are not equal due to the shape of the overlapping part of the Gaussian voltage pulses (V_{m1} and V_{nj}). This would not be the case if rectangular pulses could be used. Fig. 5 shows that the maximum image gain value can reach $\sim 2.0 \times 10^4$ while the minimum value is $\sim 1.4 \times 10^4$. Similarly, when electric pulses are applied to other input $Au-MSL_m$ of m_i (i=1–4) in turn, the four overlap areas along each $Au-MSL_m$ will also be sequentially gated.

IV. EXPERIMENTAL RESULTS

The experimental setup is shown in Fig 6. A Krypton fluoride (KrF) laser with a wavelength of 248.5 nm was used as a pulsed light source. The laser parameters were 500-fs pulse width, 5-mJ per pulse, and a repetition-rate between 1 and 5 Hz. The average energy per pulse incident on the MCP was approximately 3 mJ,

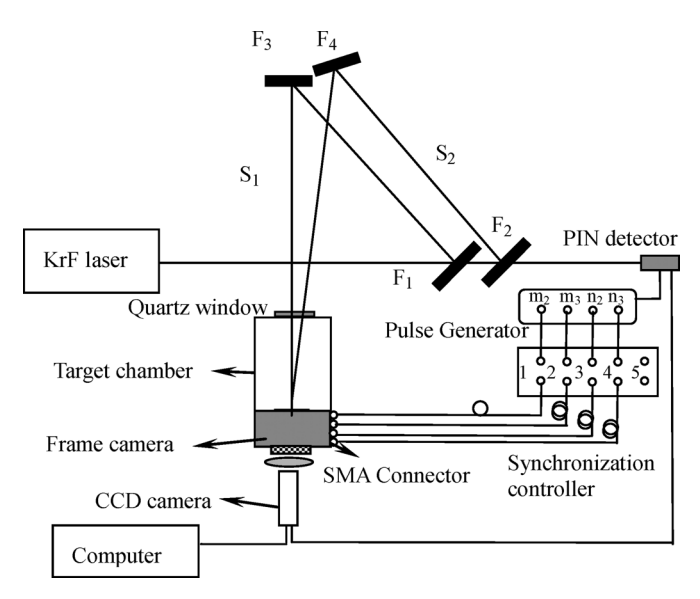


Fig. 6. Schematic illustration of the experimental setup for characterization of the orthogonal, double-gated, Chevron-MCP-XFC.

and the diameter of the laser beam at the $Au-MSL_ms$ was approximately 60 mm. The framing camera was run in a vacuum chamber with a quartz window at the front to allow optical access. The optical paths S_1 and S_2 were defined by beam splitters F_1 and F_2 and mirrors F_3 and F_4 . The mirrors were also used as an optical delay line. The delay time of a single laser pulse between S_1 and S_2 was set to one nanosecond. A PIN diode detector was used to provide trigger signals to a pulse generator which generates gating pulses for the framing camera, and a commercial CCD camera (*Pixelfly* model, manufactured by the *Cookee* Corporation, USA) was used to record the static images occurring on the phosphor screen.

Generally, a CCD camera has both external and internal trigger modes. In this experiment, we used the external trigger mode and configured the CCD camera to start recording before the high speed framing camera began to run. In this way we could capture all images occurring on the phosphor screen by selecting an appropriate trigger delay for the framing camera and exposure time of the CCD. The exposure time of the CCD camera was adjustable from 5 μ s to 60 ms according to need. We used a 30-ms exposure time for the CCD as this captured all of the images occurring on the phosphor screen with a good S/N ration.

An orthogonal, double-gated, chevron-MCP structure was used in the experimental framing camera. The HV pulse generator used contains an electronic delay which can provide an output delay for every gating pulse with an adjustable range from 0 to 1 s in 1-ns steps. However, it could only produce two negative and two positive ps-level HV pulses in a single sequence. Thus, we used only two input and output strips as shown in Fig. 7.

The negative gating pulse $V_{m2}(t)$ applied to the input side of the MCP_1 was synchronized with the laser using a synchronization controller (see Fig. 6), provided a variable delay from 0–5 ns with 20-ps steps. In addition, the delay time could also be adjusted by changing the length of coaxial-cable connecting the pulse generator and the frame camera.

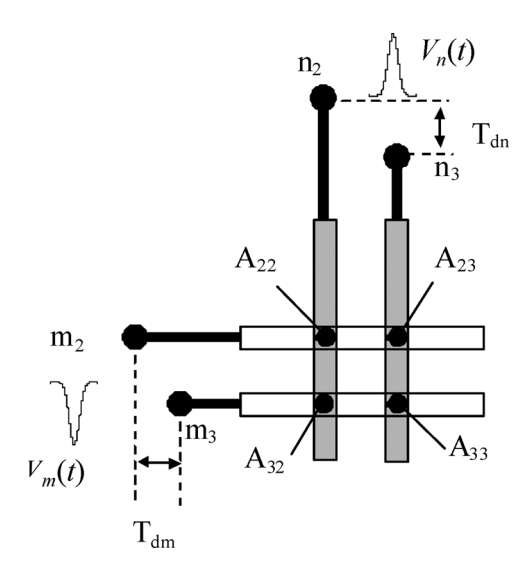


Fig. 7. Schematic illustration of the gated image areas in the experiment and the application of the gating pulses.

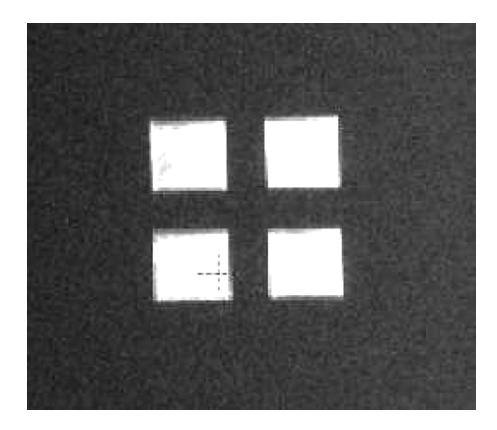


Fig. 8. Static laser images generated by the XFC.

In the experiment, we first checked the gain performance of the framing camera. A negative DC voltage was applied to both MSLs m_2 and m_3 while a positive DC voltage was applied simultaneously to MSLs n_2 and n_3 . The voltages were varied from 200 V to 600 V. The resulting static laser images recorded by the CCD camera are shown in Fig. 8, indicating that the camera has adequate gain and uniformity when -500 V were applied to MCP_1 and 450 V were applied to MCP_2 .

The temporal performance of the system was tested by applying two negative pulses $V_m(t)$ (FWHM = 250 ps, V_{mp} = -2 kV) to MSLs $\rm m_2$ and $\rm m_3$, and two positive pulses $V_n(t)$ (FWHM = 2.3 ns, V_{np} = +1 kV) to MSLs $\rm n_2$ and $\rm n_3$. The shapes of both gating pulses are shown in Fig. 9, and the resulting gated images are shown in Fig. 10.

To demonstrate the system performance, the CCD camera trigger has to be synchronized with the arrival at the area A_{22} of both the laser pulse S_1 and the gating pulses $V_{m2}(t)$ and $V_{n2}(t)$. This was done by adjusting the optical delay line formed by mirrors F_1 and F_3 and/or varying the initial trigger time for the gating pulse. When properly synchronized, the appropriate area is gated and an image appears on the phosphor screen to be recorded by the CCD camera. The resulting picture is shown in Fig. 10(a).

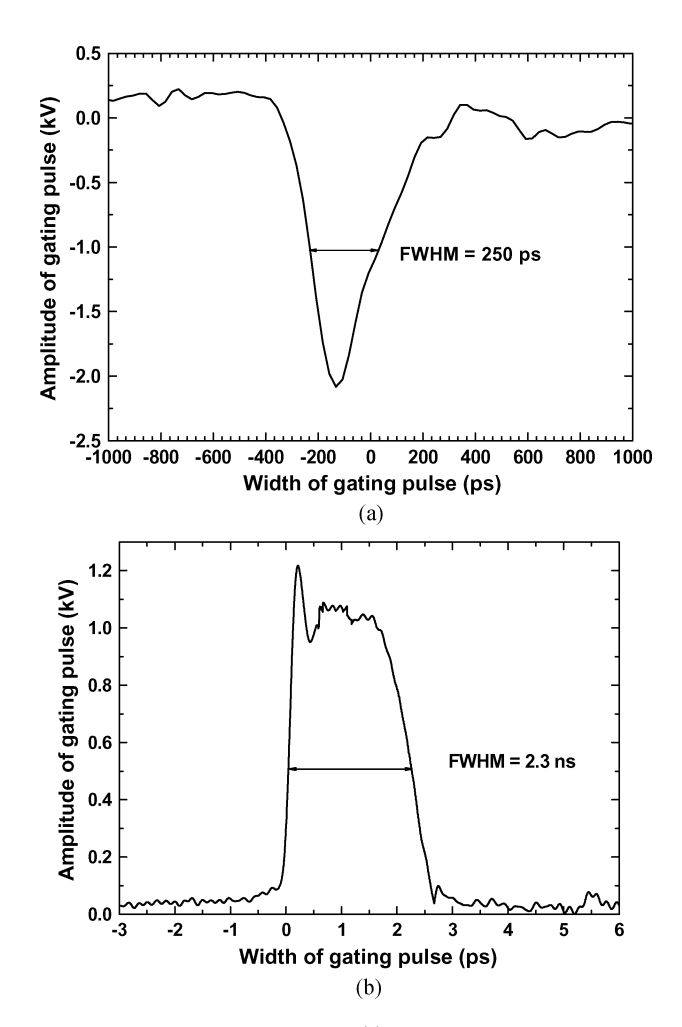


Fig. 9. (a). Negative gating pulse $V_m(t)$ (FWHM = $250~{\rm ps},~V_{mp}=-2~{\rm kV}$). (b). Positive gating pulse $V_n(t)$ (FWHM = $2.3~{\rm ns},V_{np}=+1~{\rm kV}$).

In a real application, the object to be investigated is a transient phenomenon lasting much longer than the exposure time of the XFC. In this case, we have to preset just the gating pulse widths and the delay times between them to synchronize them appropriately and thus gate the desired area of the MSL. We simulated this by using a laser with a pulse width of 500 fs and a repetition frequency 5 Hz as an object. Furthermore, we had to illuminate the next area to be gated when selecting the widths of the row and column gating pulses and delay times between them. In the experiment, we used the mirrors F_1 and F_2 as beam splitters to create two laser pulses (as shown in Fig. 6). The delay time T_{dm} between the laser pulses S_1 and S_2 was set to 1 ns by adjusting the light delay line.

We set the time delay T_{dm} between $V_{m2}(t)$ and $V_{m3}(t)$ to be greater than 1 ns. By adjusting the synchronization controller or the length of coaxial-cable we allowed $V_{m2}(t)$ to propagate to the middle of MSL_{m2} . Thus, either area A_{22} or A_{23} was gated while illuminated with the S_1 laser pulse. The results indicated whether S_1 was synchronous with the gating pulse generator and the CCD camera. Two resulting CCD images, separated by 200 ms with the laser operating at 5 Hz, are shown in Figs. 10(a) and (c).

We then set the time delay T_{dm} to be the same as the delay time between the S_1 and S_2 laser pulses. In this configuration,

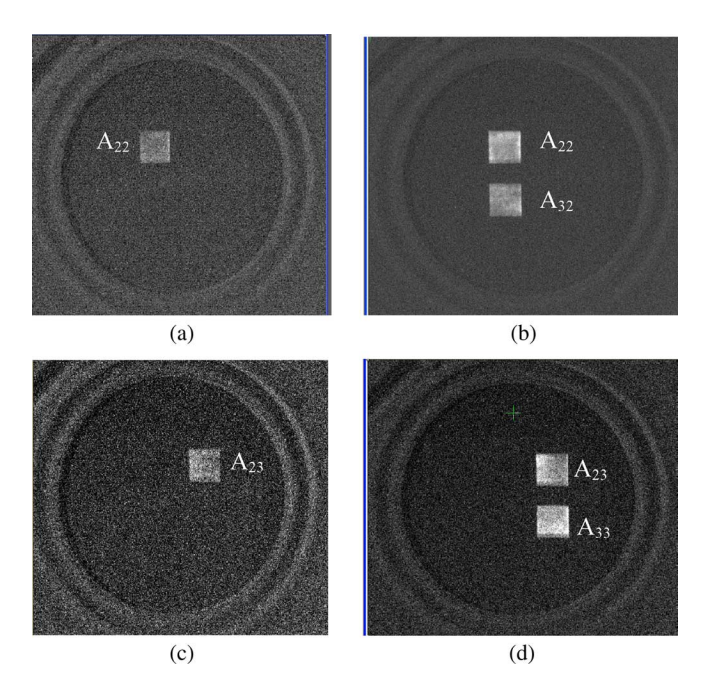


Fig. 10. XFC Phosphor screen images captured by CCD. The images were taken with $V_m(t)$ (FWHM = $250~{\rm ps}, V_{mp} = -2~{\rm kV}$), $V_n(t)$ (FWHM = $2.3~{\rm ns}, V_{np} = +1~{\rm kV}$), $T_{dm} = 1~{\rm ns}$, and $T_{dn} = 200~{\rm ms}$. Fig. 10(a) and Fig. 10(c): the synchronization states of every unit are firstly determined at gating the area A_{22} or A_{23} with $T_{dm} > 1~{\rm ns}$ and $T_{dn} = 200~{\rm ms}$. Fig. 10(b): the delay time T_{dm} between gating pulses for the areas A_{22} and A_{32} is set to be the same as the delay time between laser pulses S_1 and S_2 (i.e., 1 ns) and two exposure areas can be recorded by the CCD camera in a single image. Fig. 10(d) is similar to Fig. 10(b), but the delay time $T_{dn} = 200~{\rm ms}$.

during a single CCD camera image acquisition period, the areas A_{22} and A_{32} are gated during illumination by S_1 and S_2 laser pulses, respectively, which are separated by 1 ns. The resulting CCD image is shown in Fig. 10(b). Similarly, the areas A_{23} , and A_{33} of the MSL n_3 were gated to image the next laser pulse, 200 ms later, and the resulting CCD image is shown in Fig. 10(d).

By varying the width of the gating pulses and the delay time between gating pulses, images from different areas corresponding to different times may be acquired by the framing camera. Thus snapshots in time with a dynamic process that may evolve from nanoseconds to microseconds (or even longer) are obtained.

We can thus acquire images at any stage of the dynamic phenomena to be observed simply by controlling the various MCP-XFC parameters such as T_{dm} , T_{dn} , the initialization time of the gating pulse, or the synchronization states of the laser, the gating pulse, and the CCD. The camera performs the same as a single-gated MCP-XFC [4], [6], [7], if a DC voltage is applied to all of the vertical micro-strip lines and a gating pulse is applied to the horizontal micro-strip line.

V. DISCUSSION

We performed an experiment to verify whether or not the high speed framing tube works as expected. As a proof of concept, the result is affirmative, but several caveats apply. For instance, the laser width is too short to act as a real X-ray object that might be investigated using an XFC, while the camera itself is not a complete prototype. Most importantly, however, is that by selecting suitable T_{dm} , T_{dn} , and the widths of $V_m(t)$ and $V_n(t)$, it is possible to flexibly acquire images at any stage of the dynamic phenomena under observation.

We believe that the different intensities of the images in Fig. 10(a)–(d) are attributed to the different shape of the overlapping sections of the Gaussian electric pulses (see Section III).

It is possible to obtain images of an object at different times with the same intensity. To do this, one forms images from an X-ray-emitting object on the MSL's intersecting areas using a pinhole array and then applies a large-width rectangle wave or a DC voltage to a MSL on one MCP of the Chevron-MCP structure and apply several small-width rectangle waves with appropriately varying delay times to the MSLs on the other MCP of the Chevron-MCP structure.

While the synchronization was very important and quite difficult for this experiment, it is expected to be easier for an integrated prototype. In this proof of concept experiment, a pulse laser was used for simplicity instead of an X-ray-emitting object. However, any object emitting X-rays can be investigated by this camera.

The CCD camera is used to record the static images occurring on the phosphor screen. It should be synchronized with the high speed XFC but the synchronizing precision is not strict, because those phosphor images will last on the screen for nanoseconds to microseconds depending on the afterglow duration of the phosphor screen.

For simplicity the prototype tested had only four MSLs on each surface of the MCP, but it can be equipped with more if necessary.

VI. SUMMARY

This study demonstrates a prototype X-ray framing camera incorporating a double-gated Chevron-MCP with orthogonal MSLs on input and output surfaces, respectively. This novel type of XFC can acquire some images using exposure times that range from picoseconds to microseconds (or even longer). The advantage of this camera is that the time at which the image is acquired and the exposure time can be independently controlled by selecting suitable T_{dm} , T_{dn} values (that are independent of the propagation velocity of the gating pulse along the MSL) and the widths of the gating pulses $(V_m(t))$ and $V_n(t)$. The tradeoff is that synchronization of this camera is more complicated than for a single gated MCP X-ray framing camera.

In short, the camera is versatile, has a high gain, and a variable exposure time. It can be used to acquire time-resolved sequences

of two-dimensional X-ray images, providing a new capability to the family of high speed X-ray imaging technologies.

ACKNOWLEDGMENT

It is with pleasure, the authors would like to acknowledge the technology supporting of Dr. Jinshou Tian and Yongsheng Zhang (engineer). Thanks also to Dr. Klaus Ziock for his very valuable advice on this paper.

REFERENCES

- B. K. F. Young, R. E. Stewart, J. G. Woodworth, and J. Bailey, "Experiment demonstration of a 100-ps microchannel plate framing camera," *Rev. Sci. Instrum.*, vol. 57, no. 11, pp. 2729–2732, Nov. 1986.
- [2] J. D. Kilkenny, P. Bell, R. Hanks, G. Power, R. E. Turner, and J. Wiedwald, "High-speed gated x-ray images," *Rev. Sci. Instrum.*, vol. 59, no. 8, pp. 1793–1796, Aug. 1988.
- [3] F. Ze, R. L. Kauffman, J. D. Killkenny, J. Wielwald, P. M. Bell, R. Hanks, J. Stewart, D. Dean, J. Bower, and R. Wallace, "A new multi-channel soft x-ray framing camera for fusion experiments," *Rev. Sci. Instrum.*, vol. 63, no. 10, pp. 5124–5126, Oct. 1992.
- [4] D. K. Bradley, P. M. Bell, J. D. Kilkenny, R. Hanks, O. Landen, P. A. Jaanimagi, P. W. McKenty, and C. P. Verdon, "High-speed gated x-ray imaging for ICF target experiment," *Rev. Sci. Instrum.*, vol. 63, no. 10, pp. 4813–4817, Oct. 1992.
- [5] B. H. Failor, D. F. Gorzen, C. J. Armentrout, and G. E. Busch, "Characterization of two-gated microchannel plate framing cameras," *Rev. Sci. Instrum.*, vol. 62, no. 12, pp. 2862–2870, Dec. 1991.
- [6] A. Denysenko, S. Alexandrou, C. C. Wang, D. K. Bradley, W. R. Donaldson, T. Y. Hsiang, R. Sobolewski, and P. M. Bell, "Picosecond electrical characterization of x-ray microchannel-plate detectors used in diagnosing inertial confinement fusion experiments," *Rev. Sci. Instrum.*, vol. 64, no. 11, pp. 3285–3288, Nov. 1993.
- [7] P. M. Bell, J. D. Killlenny, G. Power, R. Bonner, and D. K. Bradley, "Multiframe x-ray images from a single meander stripline coated on a microchannel plate," in *Proc. SPIE*, 1989, vol. 1155, pp. 430–438.
- [8] B. Shan, T. Yanagidaira, K. Shimoda, and K. Hirano, "Quantitative measurement of x-ray images with a gated microchannel plate system in a z-pinch plasma experiment," *Rev. Sci. Instrum.*, vol. 70, no. 3, pp. 1688–1693, Mar. 1999.
- [9] M. T. Qiu, M. Lv, K. L. Wang, D. W. Hei, A. C. Qiu, and Z. Z. Zeng, "Time resolved X-ray image diagnostic system for Z-pinch," (in Chinese) *High Power Laser and Particle Beams*, vol. 15, no. 1, pp. 101–104, Jan. 2003.
- [10] Z. H. Chang, B. Shan, X. Q. Liu, and J. Y. Liu, "Gated MCP framing camera with 60 ps exposure time," in *Proc. SPIE*, 1995, vol. 2549, pp. 53–59
- [11] P. M. Bell, B. A. Hammel, J. D. Kilkenny, R. E. Turner, and C. L. S. Lewis, "Modeling and measurements of sub 100 ps gating with microchannel plates," in *Proc. SPIE*, 1989, vol. 1155, pp. 415–419.
- [12] E. H. Eberhardt, "Gain model for microchannel plates," Appl. Opt., vol. 18, no. 9, pp. 1418–1423, Sep. 1979.
- [13] W. B. Feller, "The dynodized microchannel plate model and secondary electron emission," *IEEE Trans. Electron Devices*, vol. ED-32, no. 11, pp. 2479–2481, Nov. 1985.
- [14] E. H. Eberhardt, "An operational model for microchannel plate devices," *IEEE Trans. Nucl. Sci.*, vol. NS-28, no. 1, pp. 712–717, Feb. 1981